Soultana Koutsoupi

Department of Physics

University of Patras , Patras -Rio , Greece

Greece 2014

Atlas Test Beam And MicroMegas Detectors

Abstract:

MicroMegas is one of the detector technologies (along with the small Thin Gap Chambers) that has been chosen for precision tracking and triggering purposes of the ATLAS muon forward detectors in the view of LHC luminosity increase. To fulfill the requirements of such upgrade, several prototype **MicroMegas** detectors were tested in recent test beam campaigns with high energy hadron beams at CERN**.** The following report describes the way that the **MicroMegas** detectors work and the procedure of the test beam at Atlas experiment at Cern .

ACKNOWLEDGMENTS

First, I would like to thank Prof.T.Alexopoulos for his kindness and his help at the short time that we had the chance to spend together at the experimental area of Atlas test beam facilities. Also , I would like to express my thankfulness to the team of Prof.T.Alexopoulos for their help and support. I had the chance to cooperate with talented, patient and passionate physicists and engineers. It was the perfect occasion to think about my future carrier and evaluate the pros and cons of being a physicist or scientist in this time of crisis.

Introduction

The Large Hadron Collider (LHC) at CERN, after the scheduled shutdown of 2017-2018, will resume its operation with a luminosity increase of five times its original design luminosity of $L = 10^{34}$ cm $^{-2}$s $^{-1}$. For the ATLAS detector ,such a luminosity increase means higher particle rates. While in most of the ATLAS muon system the detectors have enough safety margin to handle these rates, the first forward station of the muon spectrometer, called the Small Wheel, will exceed its design capabilities. The **Muon ATLAS MicroMegas Activity** (MAMMA) R&D explored the potential of the micromegas technology for its use in LHC detectors and finally proposed to equip the New Small Wheel (NSW) with micromegas detectors, combining trigger and precision tracking functionality in a single device. In middle 2013 the ATLAS Collaboration endorsed the proposal .In total, eight planes of micromegas detectors covering the full NSW will be installed, corresponding to a total detector area of 1200m^2. In addition to the micromegas, the NSW should also be equipped with eight planes of thin-gap multiwire detectors, called sTGC, such as to create a fully redundant system, both for trigger and tracking.

GAS DETECTORS

PHENOMENOLOGY OF GAS DETECTORS

Before moving on, this could be a good point to mention the main topics one will come across when studying the interactions of radiation with matter (in a gaseous detector).At the following lines is briefly described the interaction of radiation with matter.

The photoelectric effect

A photon meets an atomic (bound) electron and is absorbed, allowing for the electron to be ejected from the atom, with an energy

$$\mathbf{E = hv - EB ,} \qquad (1)$$

for hv the energy of the photon and EB the binding energy of the electron. In the energy region of the X-rays, the cross-section (per atom) is calculated

$$\mathbf{\Phi_{Photon} = 4\,\alpha^4\,\Phi_0\,(m_e\,c^2\,/hv)^{7/2}\,Z^5} \qquad (2)$$

Where α=1/137 and $\Phi_0 = 8\pi r_e^{\,2}/3 = 6.651\text{x}\ 10^{-25}\ \text{cm}^2$ (for r_e the radius of the electron) and Z the atomic number. From equation (2) emerges the strong dependence on the Z, which, depending on the application, will have a significant role on the decision for materials to be used for the detection.

An interesting point arising is what follows the emission of the electron. When ejected, the electron causes a re-arrangement in the shell, which can take either of two ways:

• the Auger effect (a radiation less transition), which is the emission of an electron of energy close to the binding energy after an internal rearrangement of the electrons on the shells, or

• fluorescence, the process through which an electron from an inner shell takes the place of the ejected electron, emitting a photon carrying the energy difference between the two shells.

Electrons

Of all the interactions the charged particles can possibly be involved in, only the electromagnetic one (Coulomb interactions, bremsstrahlung, (Cerenkov and transition radiation), whose cross section is of some orders of magnitude bigger than the rest, is practically used for their detection. In gas detectors, the ’signature’ of the particles is mainly due to Coulomb interactions.

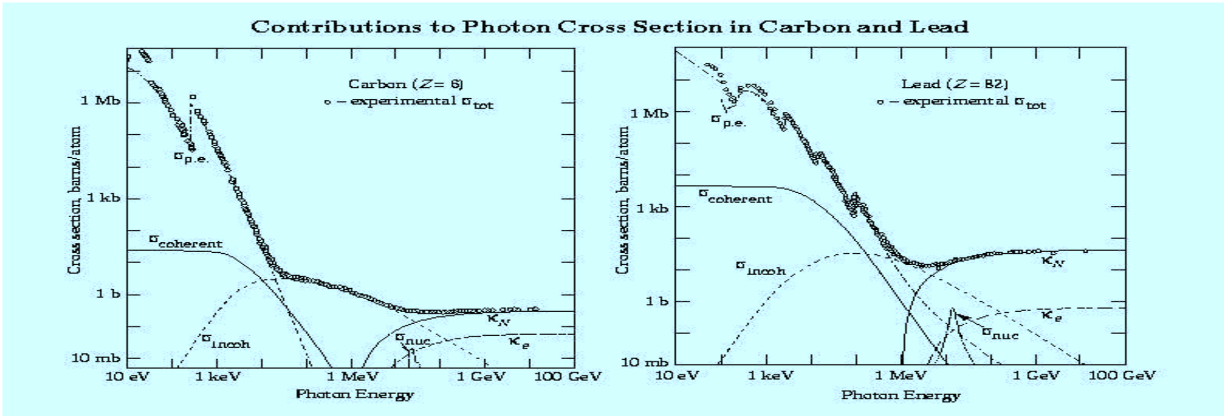

Figure [1]: The total cross-section for photon absorption in carbon and in lead. Depending on the energy of the photon, the interaction can follow different mechanisms; at low energies and up to several keV, the photoelectric conversion ($\sigma_{p.e.}$) is dominant; Compton scattering follows ($\sigma_{Compton}$), driving up to some hundreds of keV, while when the barrier of 1.22MeV is reached (2×0.511MeV) the electron-positron pair production (σ_{nuc}) is the most probable process. On the figure are noted as well $\sigma_{Rayleigh}$, for Rayleigh (coherent) scattering and K_e for the pair production in the electron field .

Energy loss due to Coulomb interactions

The basic calculation for the energy loss is given by the Bethe-Bloch formula:

$$-\frac{dE}{dx} = \frac{4\pi}{m_e c^2} \cdot \frac{nz^2}{\beta^2} \cdot \left(\frac{e^2}{4\pi\varepsilon_0}\right)^2 \cdot \left[\ln\left(\frac{2m_e c^2\beta^2}{I\cdot(1-\beta^2)}\right) - \beta^2\right] \qquad (3)$$

Where :

- C = the speed of light
- ε_0 = the vacuum permittivity
- β =v/c , e and m_e the electron charge and rest mass respectively
- $I = I_0 Z$ where I0 ≃ 10 eV (effective ionization potential of the medium)

Here , the electron density of the material can be calculated by :

$$N = (N_A\ Z\ p\ ) / (A\ M_u)$$

Where : p is the density of the material , Z its atomic number , A its relative atomic mass , N_A (6.022 × 1023 mole−1) is the Avogadro number and M_u the Molar mass constant.

The energy loss distribution

The Bethe-Bloch formula provides the mean value of the energy loss. However, due to statistical fluctuations of the number of collisions taking place finally, and on the energy transferred to each of them, the energy lost by any particle will be, most likely, different than that. Fig (4.2) shows a typical distribution of the energy loss in thin media. This Landau distribution has a very characteristic shape, that can be expressed as:

$$\mathbf{f(\lambda) = 1/ (2\pi)^{1/2} \exp(\lambda + e^{-\lambda})} \quad (4)$$

where λ denotes the normalized deviation from the most probable energy loss $(\Delta E)_{mp}$ when ΔE is the actual loss and ξ the average energy loss:

$$\lambda = (\Delta E - (\Delta E)_{mp}) / \xi \quad (5)$$

$$\xi = (4\pi / m_e c^2)(nz^2 / \beta^2)x \quad (6)$$

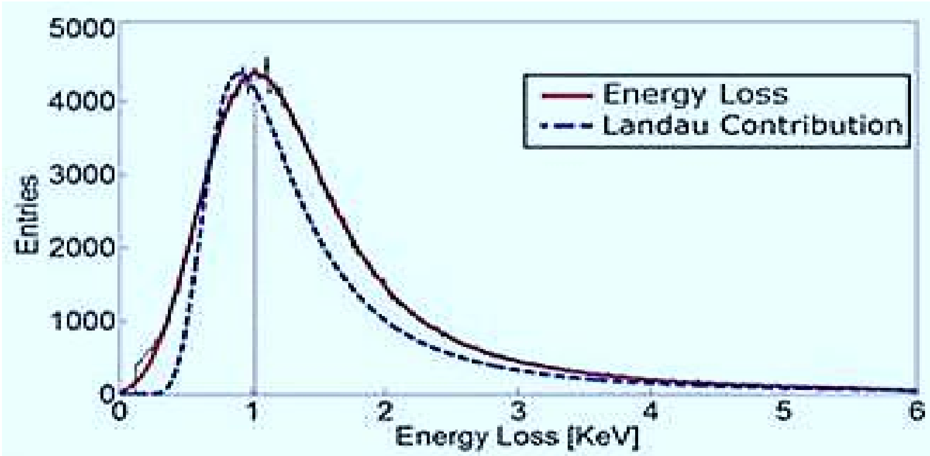

Figure [2] : The characteristic Landau distribution. The peak indicates the most probable energy loss $(\Delta E)_{mp}$. The distribution shows a tail in the high energy loss region, due to –rare– energetic δ electrons . This tail causes the mean value ξ of the energy loss to shift to the right of the peak of the distribution. The maximum allowed energy loss per collision (Emax) is shown as well.

Strangling(example) :

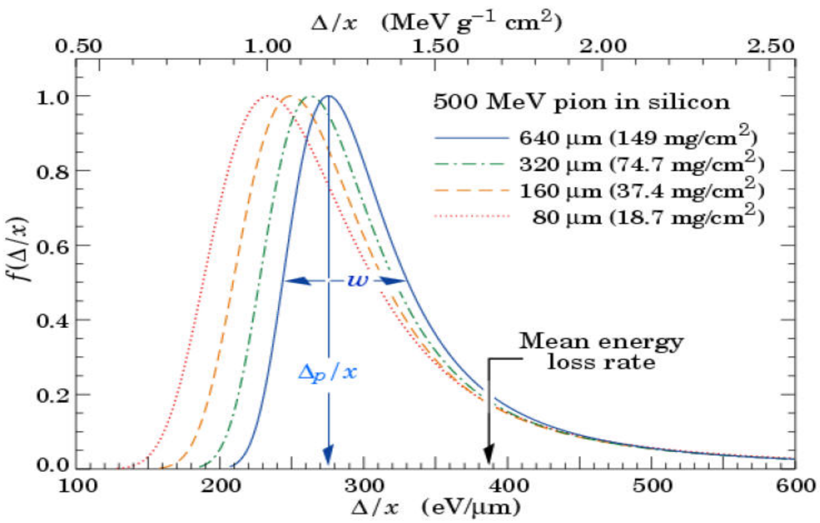

Muons

Cosmic-ray muons (μ^+, μ^-) are produced by the interaction of extra-terrestrial particles (primaries) with the Earth's upper atmosphere. Cosmic rays detected at the Earth's surface are a mixture of energetic primaries and secondaries (hard component) and lower energy secondaries (soft component). The primary flux consists of the extremely high energy (> 109 eV) protons, a-particles, and a few light nuclei. Interactions with the upper atmosphere produces a secondary flux of protons dipole moment 3.18 times that of the proton. The μ^- disappears in either of two ways; capture by a nucleus, with the emission of a neutrino(v) and a neutron(n), or by spontaneous decay to an electron and neutrino-anti-neutrino pair after coming to rest: $\mu^- \to e^- + \nu e + \nu\mu$. The probability of capture by a nucleus is small for low Z materials but increases rapidly with increasing Z. The μ^+, strongly repulsed by nuclei, have only the decay path: $\mu^+ \to e^+ + \nu e + \nu\mu$. Energy losses are by ionization until they come to rest. The subsequent decay-electron spectrum is a continuum with a shape similar to a b - spectrum, with an energy range from near zero to an end point of about 53 MeV. While the lifetimes for a μ^+ and a μ^- are the same (2.1970 ms), the measured mean lifetime in matter becomes shorter for the μ^- with increasing Z because of the competing capture by nuclei. Lifetime measurement must be examined carefully since it will most probably be a composite value for the lifetimes of both μ^+ and μ^-, neutrons, and two forms of π mesons (neutral and charged). Neutral π mesons decay quickly into photons that multiply into showers, while the charged π mesons decay to muons plus neutrinos. Muons (+ or -) carry the same charge as an electron, with a mass 206.8 times larger. Their kinetic energy is from zero to many GeV, they have a spin of ½ .

- The principal processes for energy loss are:

Inelastic collisions - with energy transferred to electrons of the material (ionization). Primary mechanism for electrons, b-rays, and muons.

Bremsstrahlung - emission of electromagnetic radiation by the decelerating particle. Principal source of energy loss for relativistic particles **$E= mc^2$** . Of minimal importance for muons because of their large mass .

Like electrons, muons are capable of transferring energy only by the electromagnetic and weak interactions, with the rate of energy loss determined by the initial energy and the Z of the material. The rate (dE/dX) drops slowly with decreasing energy to a minimum ("Minimum Ionizing"), then rises again at low energies. The "universal" value of dE/dX for " minimum ionizing " particles is: **dE/dX ~ 2 MeV/(g/cm^2)**

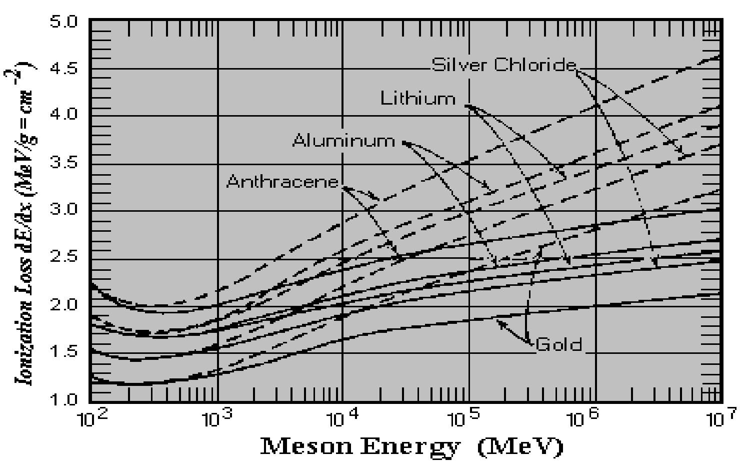

Figure [3]: Energy loss for muons in gases and solids

Excitation and Ionization in Gases

The energy loss discussed in the previous section, can be transferred to electrons through two mechanisms, excitation or ionization.

- **Excitation**

In the case of excitation, an atomic electron acquires an energy which “pushes” the atom to an elevated (excited) state

$$X + p \rightarrow X* + p$$

and is a resonant reaction, where no electron-ion pairs are produced. The atom eventually returns to its stable state, usually with the emission of a photon. A molecule may have many –characteristic– ways of excitation; for example noble gases can be excited only through photon absorption or emission, while polyatomic molecules have transitions of a rotational and vibrational nature. Excitation can result in ionization; in a gas mixture, composed by a noble gas and a quencher (a polyatomic molecules gas, usually hydrocarbons) the excited noble gas can ionize the quencher, the excitation taking place through collisions (Penning effect).

- **Ionization**

Contrary to excitation, an ionization takes place, when an electron-ion pair is created. For this to happen, the energy of the passing particle should be above a threshold equal to the ionization potential of the medium. When the ionization is caused by the incident particle itself, it is called primary ionization. If the electron of the pair gains an energy above the threshold it ionizes further, and produces secondary ionization. This phenomenon may continue until the threshold for ionizing reactions is reached. Although there is no simple way of calculating the number of primary ionization pairs produced, it is roughly linearly increasing with the average atomic number of the gas (with the exception of Xe).

Table [1]: Properties of gases at normal conditions: density ρ, minimal energy for excitation E_{ex}, minimal energy for ionization E_{ion}, mean effective ionization potential per atomic electron $I_0 = I/Z$, energy loss Wi per ion pair produced, number of primary ion n_P and total number of ion pairs nT per centimeter of path for minimum ionizing particles.

Gas	**Z**	**A**	**P [cm2 /s]**	$E_{ex[eV]}$	$E_{ion[eV]}$	$I_{0[eV]}$	$W_{i[eV]}$	$n_{T[cm-1]}$	$n_{p[cm-1]}$
H_2	2	2	8.38×10^{-5}	10.8	15.9	15.4	37	5.2	9.2
He	2	4	1.66×10^{-4}	19.8	24.5	24.6	41	5.9	7.8
Ar	18	39.9	1.66×10^{-3}	11.6	15.8	15.8	26	29.4	94
Xe	54	131.3	5.49×10^{-3}	8.4	12.1	21.1	22	44	307

ΔE is the energy lost and Wi the effective energy for the creation of one electron-ion pair. Values for Wi and other gas properties are given in Table [1]. For gas mixtures the former formula takes the form :

$$n_T = \sum (\Delta E/W_i) \times q \qquad (7)$$

where i indicates each component, and q the percentage of the component in the mixture.

Transport of ions and electrons in gases

The number of pairs created has just been calculated, and yet that is not necessarily the number of pairs that will be detected; recombination or electron attachment might take place. In the absence of an external electric field (or when it exists but is a low one), the electron-ion pairs will be recombined, drawn to each other by their electrical attraction, and will emit a photon, a process depending on the electron and ion concentrations. In the presence of electronegative gases, the electrons might be captured by atoms of the gas before they are collected, releasing energy known as electron affinity. The probability of attachment h, is very high for oxygen and practically zero for noble gases.

Diffusion

When no electric field is present, the electrons and ions produced by passing radiation lose their energy rather soon, because of the multiple collisions with the gas molecules. They will rest when they assume the average thermal energy :

$$E_T = 3/2\ kT$$

where k is Boltzmann's constant and T the temperature, while their speed will be (if their mass is m):

$$u = (8kT/\ \pi m)^{1/2}$$

Naturally, the electrons will be much faster than the ions, due to their much smaller mass.
After diffusing for time t, the linear distribution of the charges is given by:

$$dN/dx = N_0(4\pi Dt)^{(-1/2)}\exp\{-\chi^2/(4Dt)\} \quad (8)$$

where N_0 is the total number of charges, χ the distance from the origin and D the diffusion coefficient. The standard deviation then, is expressed using the diffusion coefficient by:

$$\sigma(\chi) = (2Dt)^{1/2} \quad (9)$$

*for three dimensions the standard deviation is $\sigma(\chi) = (6Dt)^{½}$

With the help of the kinetic theory, and assuming a classical ideal gas, the expression:

$$D = \{2/(3(\pi)^{½})\} x\, (1/P\,\sigma_0)\, x\{(kT)^3/m\}^{1/2} \quad (10)$$

(defining σ_0 as the total cross section for a collision with a gas molecule, P and T the pressure and temperature, respectively, of the gas) gives the diffusion coefficient and shows its dependence on the various gas parameters.

Multiplication

A single electron drifting towards an anode wire in a strong magnetic field, carries some energy ǫ given by equation. As it was discussed before, for moderate electric fields the energy carried by the electron will be rather constant on average, due to the random collisions with the gas molecules. However, for higher fields –in the time between collisions with the gas molecules– its energy may increase over the first ionization potential of the gas, and an electron-ion pair will be produced, while the first electron continues its travel possibly producing more pairs. In the same way, these secondary electrons can produce further ionization forming finally an avalanche. As already noted, the mobility of the electron is much greater than that of the ions, therefore the electrons are the front of this cloud of charges, while the newly produced ions are still close, parting towards the first produced ions at their pace; the result of this movement is a drop-like distribution as shown in the schematic of figure[4].

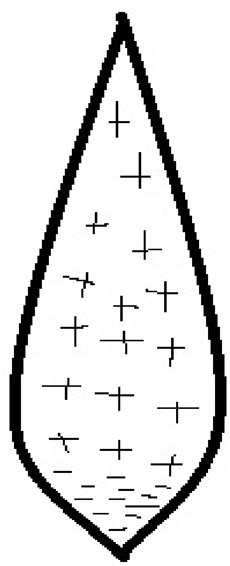

Figure[4] : The drop-like shape of an avalanche; the more mobile electrons take the head of the drop, leaving behind the slower ions, which are drifting upwards.

The distance that this electron will travel until ionization defines the mean free path for ionization. Probably the most interesting quantity is the first Townsend coefficient α, the inverse of the mean free path of ionization. α represents the number of pairs produced per unit length of travel. If at some point there are n electrons, after they drift for a path dx

$$dn = n\alpha dx \quad (11)$$

new electrons will have been produced, hence the total number of electrons created in a path x is:

$$n = n_0 e^{\alpha\chi}$$

The multiplication factor or gas gain M is then given by:

$$M = n / n_o = e^{\alpha\chi} \qquad (12)$$

This factor cannot be increased at will, eventually a spark breakdown will occur. The Raether limit, the limit for multiplication before breakdown is :

$$\alpha x \sim 20 \text{ or } M \sim 108$$

In practice the gain achieved is usually two orders of magnitude less than the Raether limit.

The basic operation of the gas detectors, is the avalanche multiplication.

MicroMegas Gaseous Detector

In particle physics there is a large variety of detectors using different materials and based on different technologies. For example, some of them are solid detectors, semiconductor detectors (silicon or germanium) or scintillation detectors. **MicroMegas** detectors [5] belong to a particular sort of particle gaseous detectors.

MICROMEGAS is a high gain gaseous detector, which can stand up alone without a need of an additional preamplification. It combines high accuracy, high rate capability, excellent timing properties and robustness. Invented in 1992 by Georges Charpak and Ioannis Giomataris , the Micromegas are mainly used in experimental physics, in particular in particle physics, nuclear physics and astrophysics for the detection of ionizing particles. A particle detector is used to detect a passing particle and obtain information such as its position, arrival time and momentum. In experimental physics, the particle is usually coming from a particle accelerator but it can also come from space (cosmic ray) or from nuclear reactor. The **MicroMegas** detector, as every gaseous detector , detects particles by amplifying the charges that never have been created by ionization in the gas volume . In **MicroMegas** detector , this gas volume is divided in two by a metallic micro-mesh placed between 25μm and 150μm of the readout electrode(strips).The micro-mesh is the key element since it allows, at the same time, a high gain of 10^4 with and a fast signal of 10ns.

Detector Description

Its operating principle can easily being described through its elements; figure [5] shows a schematic view:

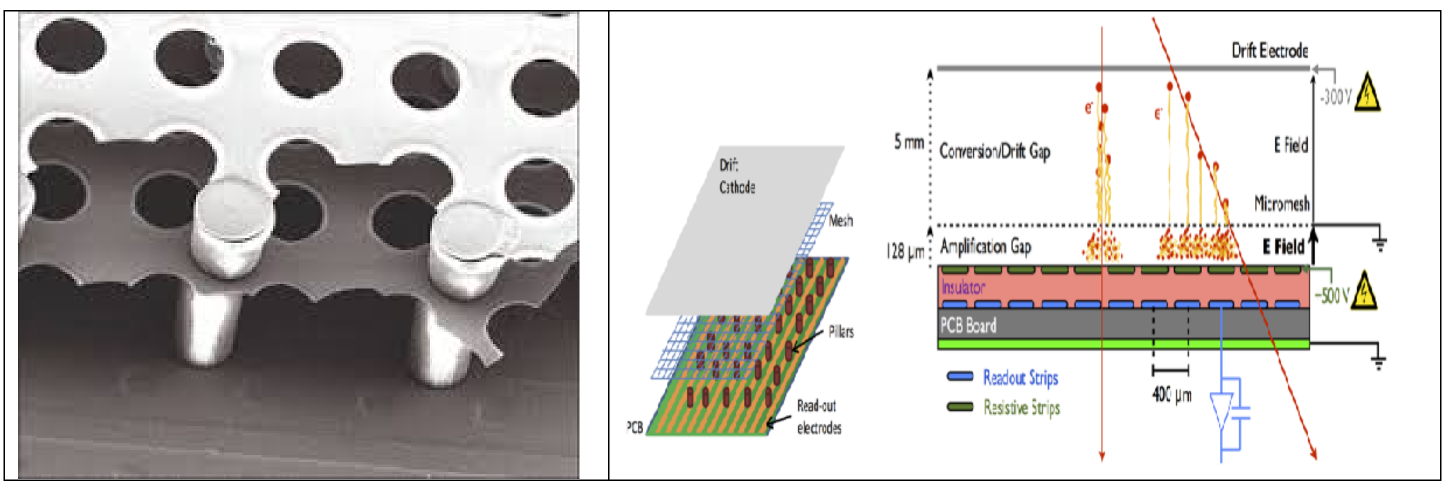

Figure [5]: A schematic view of **MicroMegas**: the micromesh separates the detector volume to the conversion gap (**5**mm) and the amplification gap (of the order of **128**μm) which ends to the strip plane. Also between the micromesh and the strip plane, there are pillars which are at this position as a base for the micromesh (the pillars are made of polyamide). The ratio of the gas to the detector is 93% Argo and 7% carbon dioxide.

The very first part a particle will have to cross is the drift electrode. As soon as the drift electrode is passed, the particle is already inside the conversion region, which stretches up to some mm until the grid. It holds a rather weak electric field –of the order of 1 kV/cm (in particular is 600V/cm) – and is the place where the ion-electron pair production takes place. The role of the grid (or else micromesh) is multiple, and does more than marking the end of the conversion gap and the beginning of the amplification one. It is made out of copper (5 μm) with a process which relies on the photolithography technique that allows to print on it 25 μm openings and a pitch of 400 μm. The voltage applied to it (up to 500V) is such that the ratio of the electric field in the amplification gap over the field of the conversion gap is very big. The bigger the ratio the higher the electron transmission to the amplification gap reached (in practice a ratio of 20 means full transmission). Once in the amplification gap, the process of avalanche is easily started; the gap is so small (of the order of 128 μm) that the electric field achieved is very high (up to 40 kV/ cm , in particular is 42kV/cm). At the same time as providing a smooth way for the electrons into the amplification gap, the micromesh prevents the ions produced by the avalanche to enter the conversion gap.

While the ions are collected by the micromesh with a high efficiency and speed, the electrons continue in the amplification gap and end their travel on the anode electrode. The anode electrode consists of copper strips with a typical width of 100 μm and a pitch of 400 μm, grounded through low-noise charge preamplifiers of high gain to an isolating layer (usually kapton).

<u>The advantages of the technique introduced with MicroMegas are listed below:</u>

- The fast response: because of the very small path the ions need to travel (amplification gap length $\sim$ 128 μm) and of the very strong field, the ions are very rapidly collected, suppressing any space-charge effects.

- Any mechanical imperfection on the stretching of the micromesh above the strips is compensated, leading to essentially steady gain; an approximation of the change in the amplification factor M with the amplification gap d is given by :

$$\delta M / M = \alpha d\ (1 - Bd/V)\ (\delta d/d) \quad (13)$$

For pressure P, applied voltage V and B a constant depending on the gas used. Under constant pressure, when d decreases, the multiplication factor increases up to a maximum (for d = V/B) and then decreases for higher values of d. The combination of the amplification gap and the applied voltage in the **MicroMegas** detectors is such, that the multiplication factor is maximized, so fluctuations due to defects of flatness between the mesh and the anode plane are canceled.

- Because of the constant field along the amplification region, the signal detected in the anode is equally due to the ions and the electrons, contrary to the wire chambers.
- An excellent spatial resolution.
- Counting capability of the order of 10^6 counts $mm^2\ s^{-1}$ due to the fast evacuation of the ions and the high granularity of the mesh.

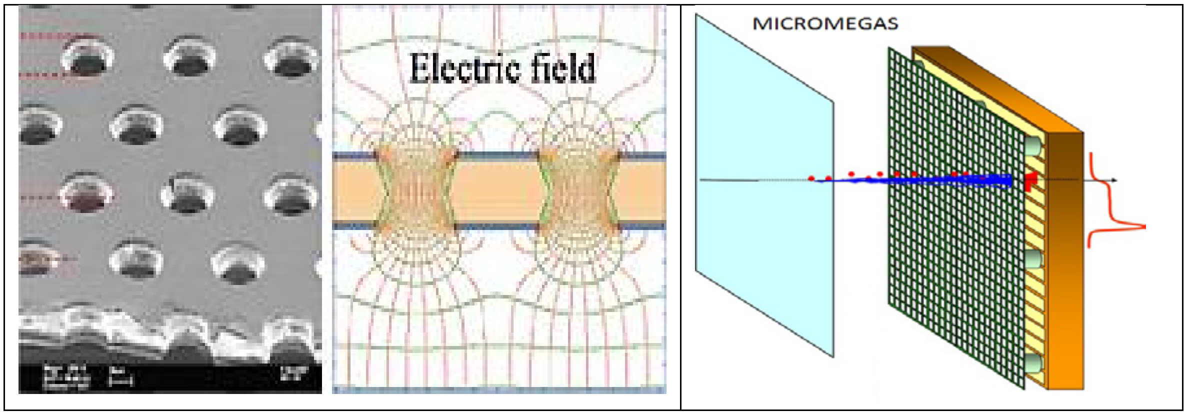

Figure [6]: Left: A schematic representation of the passage of one particle through the detector's volume. Right: The electric field lines starting just above the mesh and resulting on the strips.

Deeper Description of the detector MicroMegas

In the beginning of 2013 two large 1x2.4m^2 (0.92 x 2.12m^2 active area) **MicroMegas** detectors were build. The readout panel is composed by four **micromegas** boards of 0.5mm thick glued together to an aluminum plate that served as a stiffening panel. The total number of strips are 2 x 2048. On top of the resistive strips 128μm high pillars were deposited every 4 mm, following the same procedure as used in the bulk process. On the drift panel the "inner" skin serves as drift electrode while on the same skin, a 5mm high frame is fixed to which the mesh is glued. When the chamber is closed the mesh, that makes the ground contact, sits on the 128μm high pillars. When HV is applied to the resistive strips the electrostatic force between mesh and resistive strips ensures that the mesh is in good contact with the pillars. Data taken with the chamber in the test beam show an excellent performance with clean signals and a homogeneous response over the full area of the detector. Figure[7] shows the detector on the assembly and testing phases while the figure [8] shows the homogeneity over its surface.

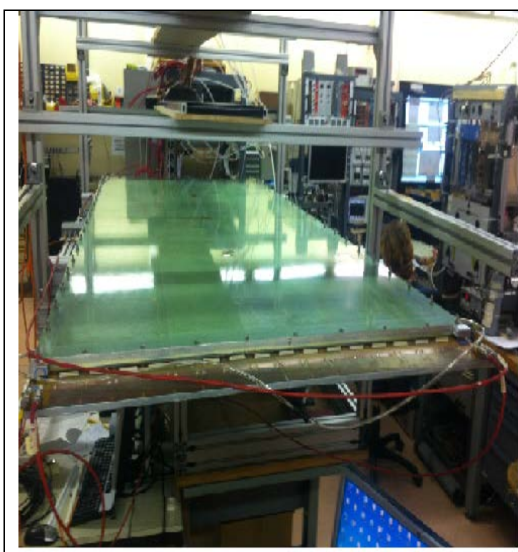

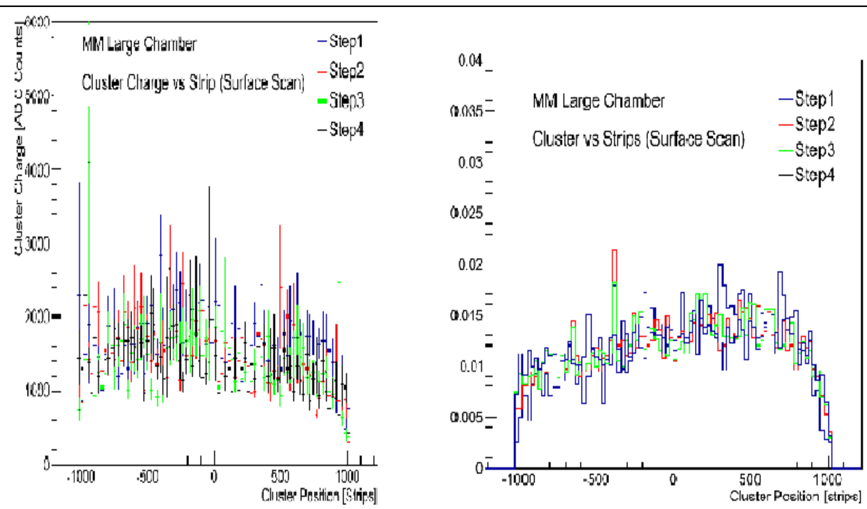

Figure[7] : The large prototype sitting on the cosmic stand at the CERN RD51 lab. **Figure[8]:** The reconstructed cluster charge (left) and position(right) over the full detector surface

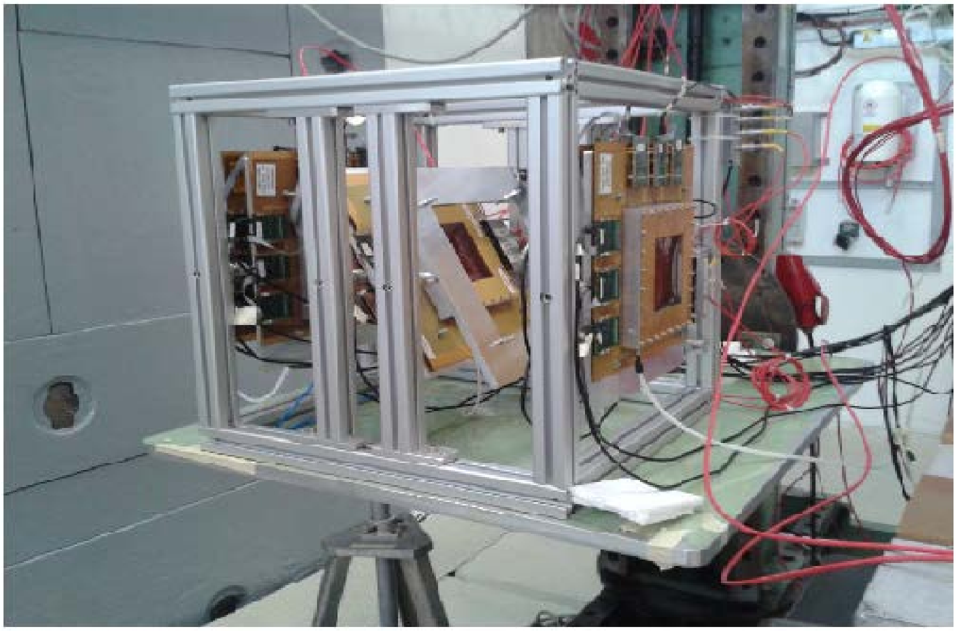

Performance

MicroMegas detectors of an active surface of 10 x10 cm^2 have been tested during test beam campaigns at CERN with high momentum hadron beams. Using those detectors with a strip pitch of 400 µm a spatial resolution of 65 µm was easily achieved for perpendicular tracks. Since the NSW will be located in the ATLAS experiment tracks between 10^0 – 30^0 are expected, studying the performance with inclined tracks is of particular interest.

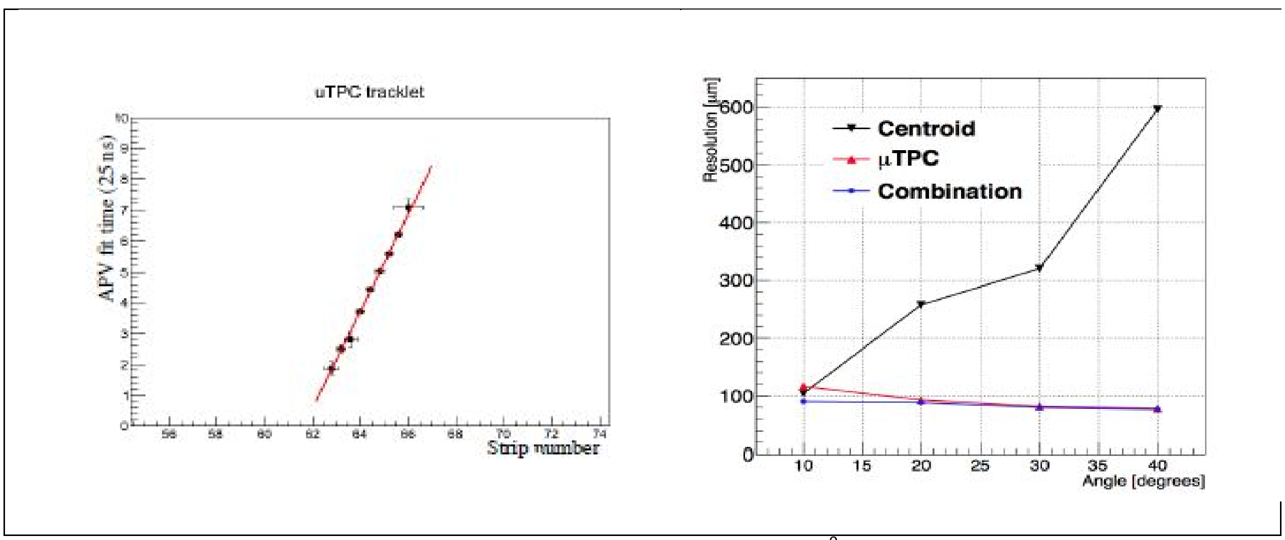

Figure [9]: On the left a reconstructed track in the 5mm drift gap under 30^0. On the right plot the spatial resolution versus the incident track angle with diferent reconstruction techniques.

The µTPC Scheme

Measuring the arrival time of the ionized electrons with a time resolution of a few nanoseconds allows reconstructing the position of the ionization process and thus reconstruction of the particle track in the drift gap of the detector. With the Ar:CO_2 (93:7) mixture and an electrical drift field of 600V/cm the drift velocity is 4.7 cm/µs, corresponding to a maximum drift time of about 100 ns for a 5mm drift gap. Figure [9] shows an example for a reconstructed track traversing the detector under 30^0 and the spatial resolution as a function of the incident track angle using the µTPC mode. An analysis technique that combines the reconstructed µTPC and charge centroid points, improves the spatial resolution especially for particle tracks of around 10^0, while results in a homogeneous spatial resolution under 100 µm along different track angles.

Performance of the MicroMegas with high energy particle beams

- **CERN H6 experimental hall—setup and operating conditions**

The reported results are based on the test beam data collected in July 2012 at the SPS H6 beam line. The beam was composed of 120 GeV/c pions with a particle rate between 5 and 30 kHz and transverse dimensions of ~ $2cm^2$ on the chambers. Up to eight resistive **MicroMegas** (MM) test chambers (T1–T8) were aligned along the beam line. All chambers had an active area of 10 x 10 cm^2, a strip plane with 0.4mm pitch and drift gap of 5 mm. In figure [10] bellow the layout of the setup is reported. The eight chambers were oriented in a back-to- back configuration forming four doublets of **MicroMegas** with a total lever arm of 600 mm. The chambers were operated with standard Ar:CO_2 gas mixture (93:7) with different configurations of the drift and amplification electrical fields. Reference operating settings were 600 V/cm electrical drift field, with a drift velocity of 47 mm/ns, and an amplification voltage of HV = 540 V.

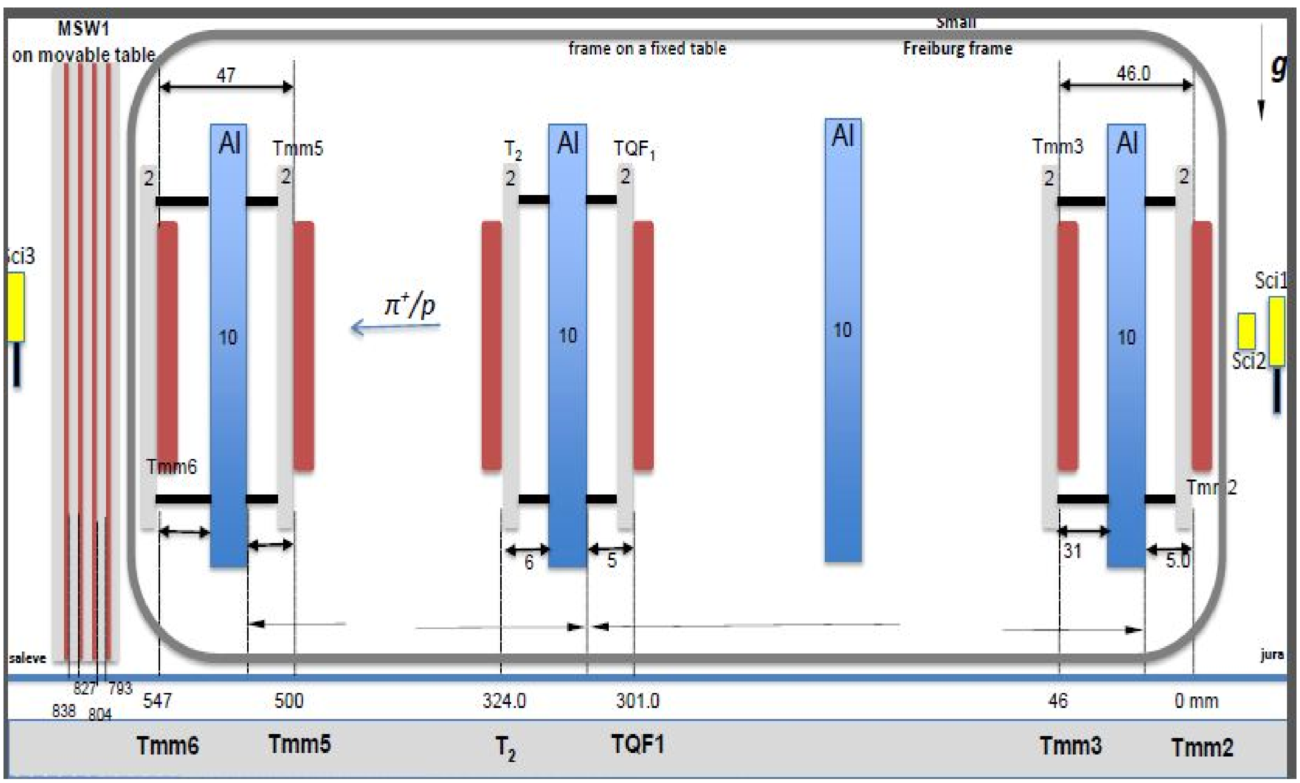

Figure[10]: Set up of the **MicroMegas** in the SP/T9 experimental area in August 2014. Install MSW1 on the movable table between TMM6 & Sci3.

Performance of the MicroMegas in a magnetic field

The MM chambers of the NSW will operate in a magnetic field with large variations and values up to about 0.3 T, with different orientations with respect to the chamber planes and a sizeable component orthogonal to the MM electric field. The effect of the magnetic field on the detector operation has been studied with test beam data and simulations. Figure [11] shows the Garfield simulations for the drift velocity and the Lorentz angle as a function of the drift electric field for several values of the magnetic field (perpendicular to electric field) and for an $Ar{:}CO_2$ 93:7 gas mixture. Figure [12] illustrates the effect of the magnetic field on a MM chamber. The drift direction of the ionization electrons is tilted with respect to the electric field direction by the Lorentz angle. Depending on the relative signs of the track angle θ_{track} and the Lorentz angle θ_L a "focusing" or "defocusing" configuration is expected, where the ionization cluster is spread over a larger (smaller) number of strips when θ_{track} and θ_L have different (same) sign. A "singular" configuration is reached when the particle track inclination is equal to the Lorentz angle $\theta_{track} = \theta_L$. From the point of view of track reconstruction, this condition is equivalent to a perpendicular track in absence of magnetic field, where the clusters have minimal spread (minimal size) and the charge weighted cluster centroid provides best spatial resolution.

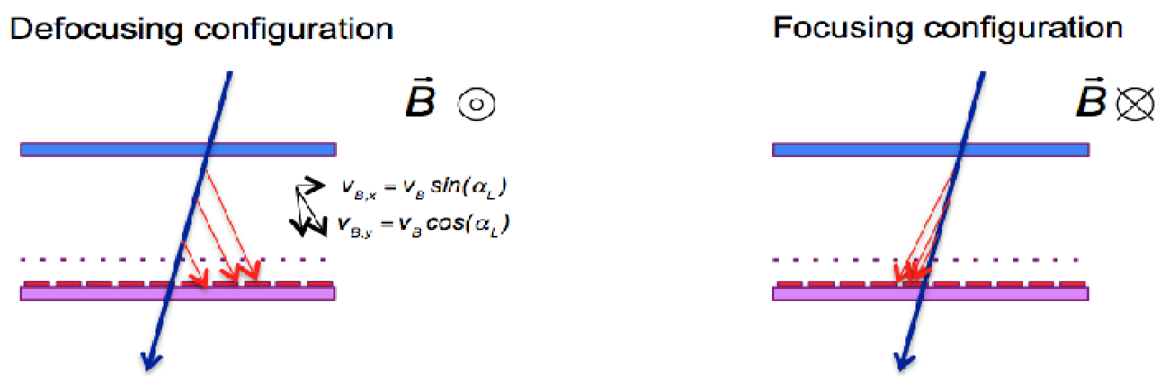

Figure[11]: Illustration of the effect of the magnetic field on the drift in a MM chamber. The electrons drift along the Lorentz angle direction. A "defocusing" (left) or "focusing" (right) configuration can be distinguished, depending on the track angle and the Lorentz angle having opposite or same sign.

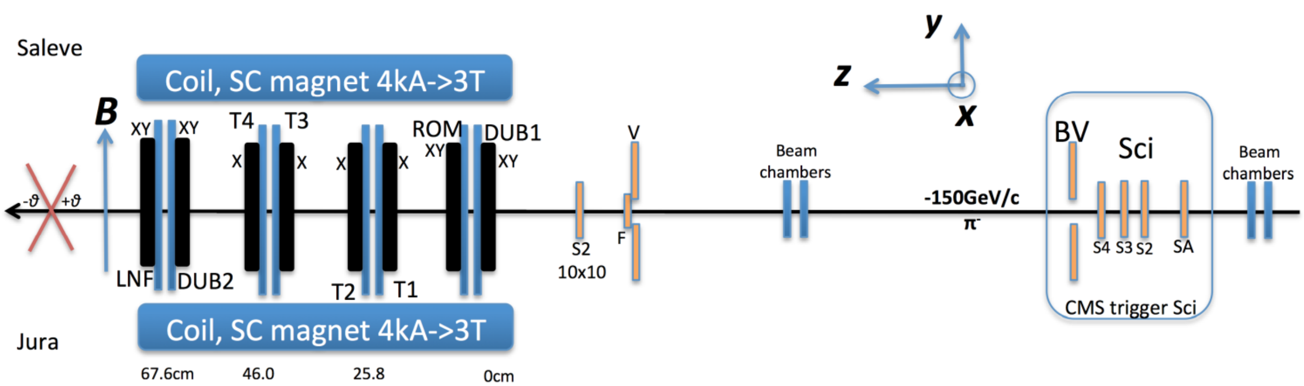

Figure[12]: Setup of the **MicroMegas** test chambers in the SPS CERN H2 experimental area in June 2012.

Readout electronics and Data Acquitition

The data acquisition system was based on the Scalable Readout System (SRS) developed by the RD51 Collaboration. The front-end electronics were based on the 128 channel APV25 ASIC in which detector signals are shaped with a CR-RC circuit and sampled at 40 MHz. In the setup the trigger was provided by the coincidence of three scintillators plus a veto. For each event, zero-suppressed data were acquired, for each strip by sampling the APV25 integrated charge signal shape. by the synchronization of the scintillator/photomultiplier trigger signal. For this reason most of the results obtained by time measurements will be reported from differences between chambers where the contribution of a global time jitter vanishes. From signal shaping analysis both time and charge information were obtained. In figure [13] a typical sampled signal from one channel is shown with a Fermi-Dirac fit function to the leading edge. Time at half height is taken as the strip time-hit, while maximum height is taken as strip charge. The time resolution was estimated from the distribution of the differences of first hit arrival time of two chambers traversed by the same particle track. In figure [14] the Gaussian fit to the distribution of the time difference of two chambers in back to back configuration, T1 and T2, has a width of 14.6 ± 0.3 ns. Assuming the same resolution for the two chambers the single chamber time resolution is 1/√2 of the reported difference width, resulting in σ_t = 10.3 ± 0.2 ns. The adopted configuration allowed to record 27 samples for a total time window of 675 ns. It should be mentioned that the APVs were operated at a frequency of 40 MHz, completely unrelated to the particle beam. Since the APV25 only accepts clock-synchronous triggers, a jitter of ± 12.5 ns, corresponding to the width of one clock cycle, is introduced

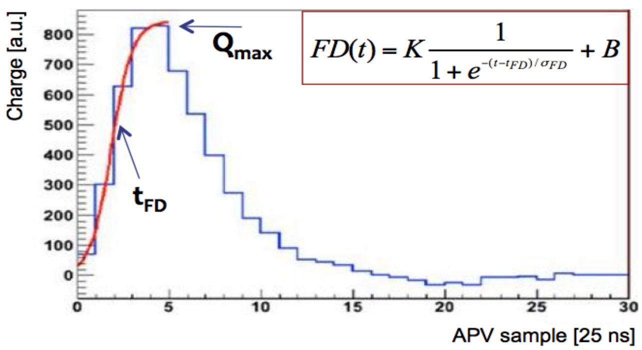

Figure [13] : A typical pulse shape from one channel (one strip) of the APV25 operated at 40MHz with 27 samples. A fit with a Fermi-Dirac function with an additional baseline is performed to determine the strip-hit- time and collected charge.

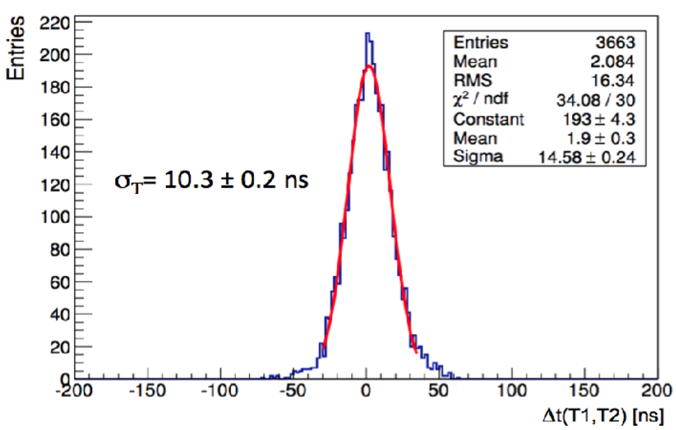

Figure[14] : Distribution of the differences of first time hits between two MM chambers in back to back configuration. The single chamber time resolution is 1/√2 times the width of the fitted Gaussian, assuming same resolution for the two chambers.

From primary ionization spatial spread, a time resolution in the order of 5–6 ns is expected. The measured single chamber time resolution of about 10 ns in the present set-up is dominated by the contributions of the electronics read-out chain, front-end and DAQ, and by the hit-time extraction method.

Triggering with MicroMegas

Micromegas detector system will contribute to the formation of the Level-1 muon end-cap trigger, forming a very powerful, redundant trigger system along with sTGC detectors. Exploiting this capability, however, requires a large number of electronics channels, about two million for an eight layer detector system. The electronics of the NSW must provide both a high resolution vector, in real time, to be used in the formation of the muon Level-1 trigger in addition to the amplitude and time information provided on the reception of a Level-1 accept. In order to reduce the number of trigger channels the design takes advantage of the **micromegas** detector's fine readout pitch to reduce the number of channels by a factor of 64 resulting in a total channel count for the trigger logic of about 33,000. This is accomplished by considering only the first arriving hit in each 64-channel front-end ASIC for a given bunch crossing (25 ns), resulting in a system with granularity of 32mm (64x 0.5 mm) but having spatial resolution better than half a millimetre by simply recording the address of the strip with the earliest arrival. This task is realized by a newly developed front-end ASIC, the VMM. Developed at the Brookhaven National Laboratory (BNL), the VMM1 (first version of the VMM family) was tested in 2012 test beam fulfilling the requirements of providing precision tracking and trigger data.

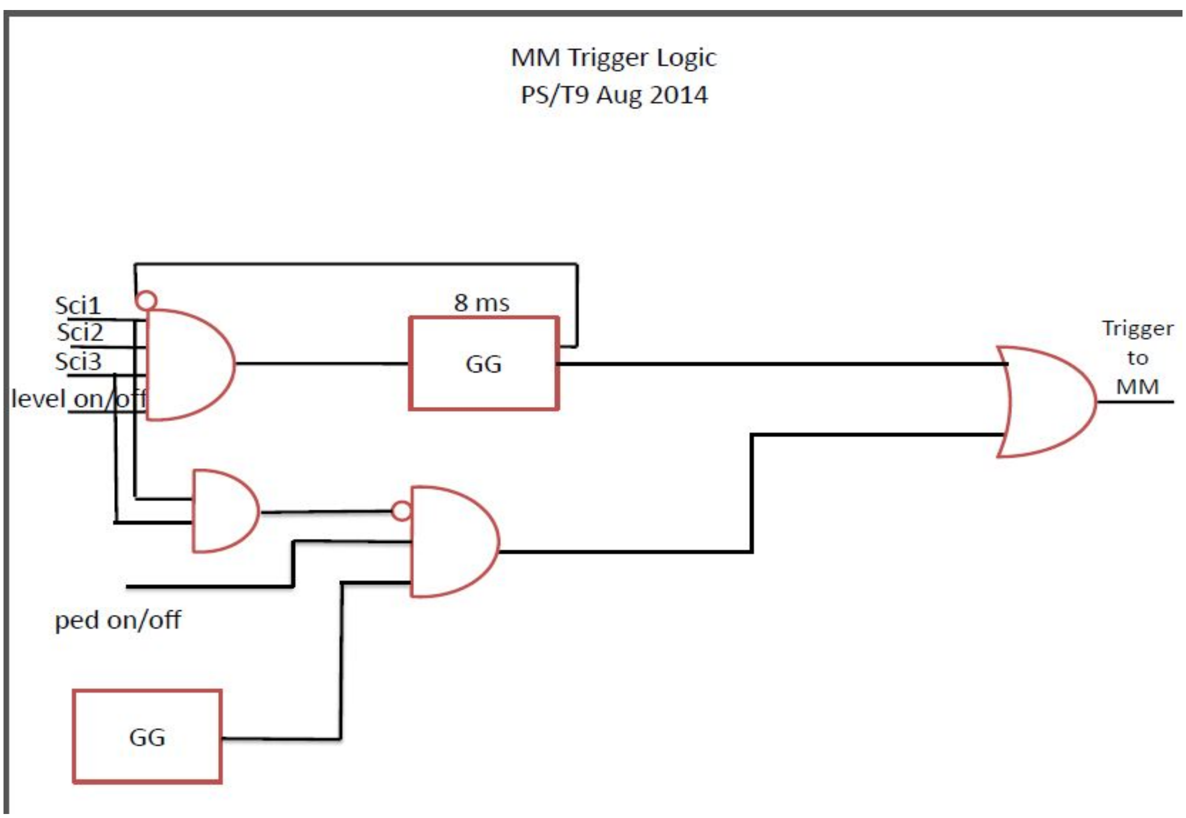

Figure[15]: MM Trigger logic at Atlas Test Beam

Table[2]: Radiation test with **MicroMegas** detectors

Irradiation with	Charge Deposit (mC/cm^2)	HL-LHC Equivalent
X-Ray	225	5 HL–LHC years equivalent
X-Neutron	0.5	10 HL–LHC years equivalent
Gamma	14.84	10 HL–LHC years equivalent
Alpha	2.4	5x108 sparks equivalent

Conclusions

In the past few years there have been performed several test beam campaigns, primarily with high energy particle beams at the Super Proton Synchrotron (SPS) beam lines at CERN, using MM detector prototypes of dimensions 10 x 10 cm^2. The aim of these tests was to evaluate the performance of the detectors under operational conditions similar to those expected for the ATLAS NSW. A selected set of the test-beam results have been reported, which constitute a small part of the huge effort of the collaboration in performance studies. Following the ATLAS schedule, 1200m^2 of **MicroMegas** detectors will be constructed and assembled on 2015–2016 while the installation and commission of the full system will follow on 2017–2018.

References :

[1]: T. Alexopoulos et al., Development of large size Micromegas detector for the upgrade of the ATLAS muon system, Nucl. Instrum. Meth. A 617 (2010) 161. http://inspirehep.net/record/1309305

[2]: For the 3rd INTERNATIONAL CONFERENCE ON MICRO PATTERN GASEOUS DETECTORS 1–6 JULY, 2013 ZARAGOZA, SPAIN /M. Iodice INFN Sezione di Roma Tre, Via della Vasca Navale, 84 — 00146 Rome, Italy http://iopscience.iop.org/1748-0221/9/01/C01017

[3]: T.Dafni , A search for solar Axions with the MicroMegas detector in Cast. http://tuprints.ulb.tu-darmstadt.de/577/

[4]: Aug 2014 testbeam @ PS/T9 07.08.2014 - 14.08.2014 Paolo, Theo Micromegas Meeting, CERN

[5]: G.Cauvin , A study of MicroMegas detectors with resistive anodes for muon reconstruction in HL-LHC. Particle Physics, Department of Physics School of Enginnering Sciences Royal Institue of Technology,Sweden Stockholm, Sweden 2012http://kth.diva-portal.org/smash/record.jsf;jsessionid=8c71daaa550b505ca96ad93391ef?pid=diva2:551264&searchId=null&rvn=2

[6]: I.Giomataris , MICROMEGAS: results and prospects, CEA/Saclay, DAPNIA,91191 Gif-sur-Yvette Cedex. France,http://www.slac.stanford.edu/pubs/icfa/fall99/paper1/paper1.pdf